PHYSICAL REVIEW B **92**, 180203(R) (2015)

Using geometry to manipulate long-range correlation of light inside disordered media

Raktim Sarma,[1] Alexey Yamilov,[2,*] Pauf Neupane,[2] and Hui Cao[1,†]
[1]*Department of Applied Physics, Yale University, New Haven, Connecticut 06520, USA*
[2]*Department of Physics, Missouri University of Science and Technology, Rolla, Missouri 65409, USA*
(Received 10 May 2015; revised manuscript received 11 October 2015; published 5 November 2015)

We demonstrate an effective approach of modifying the long-range spatial correlation for light propagating inside random photonic waveguides by varying the shape of the waveguide. The functional form of spatial correlation is no longer universal in the regime of diffusive transport and becomes shape dependent due to the nonlocal nature of wave propagation. The spatial dependence of the correlation may become asymmetric for light incident from opposite ends of the waveguide. This work opens the door to control nonlocal effects in mesoscopic transport of waves by tailoring the geometry of random systems.

DOI: 10.1103/PhysRevB.92.180203 PACS number(s): 42.25.Bs, 72.15.Rn

The diffusion model has been widely utilized to describe wave propagation in disordered media, e.g., light in biological tissues, ultrasonic waves through cracked metals, and electron wave functions in disordered conductors. It, however, ignores the interference of scattered waves, which lead to many prominent phenomena, including Anderson localization, universal conductance fluctuations, and enhanced backscattering [1–3]. Extensive theoretical and experimental studies in the past three decades have illustrated that mesoscopic transport of both classical and quantum mechanical waves is governed by wave interference effects [4,5].

One important consequence of wave interferences in random media is the correlations in the fluctuations of scattered intensities [6,7]. The interference between waves scattered along independent paths gives rise to an intensity correlation on the scale of a wavelength, where one crossing of paths generates long-range correlation beyond the mean free path, and two crossings lead to an infinite-range correlation [8,9].

The nonlocal correlations have direct consequences for the coherent control of light transmission through random media via wave-front shaping [10], which has advanced rapidly in the past few years due to potential applications to deep tissue imaging [11–13]. Indeed, focusing light on a single speckle simultaneously brightens nearby speckles, hence reducing the contrast of focusing [14,15]. It has been shown that the spatial correlation of intensity inside the random medium [16–20] determines not only focusing contrast but also energy deposition into the sample [21]. Moreover, the long-range correlation also affects the enhancement of total transmission [22] by an optimized wave front with a limited degree of input control [23]. Therefore, manipulating the nonlocal correlation can open up a new avenue to controlling waves inside random media.

Typically, the magnitude of long-range correlation is small, but it becomes significant in strongly scattering media, especially when the localization regime [3] is approached [8,9,24–27]. Experimentally long-range correlations have been observed not only in space, but also in time, frequency, angle, and polarization, but most measurements are performed on transmitted or reflected light, i.e., *outside* the random media [17,19,28–34]. Modifications of the correlations of transmitted light have been realized with two techniques: (i) varying the spot size of an incident beam on a wide disordered slab [16,19,26], and (ii) inserting a constriction, e.g., a pinhole, inside a random medium [30,35]. However, the possibility of manipulating long-range correlations *inside* the random media has not been explored. This is at least in part due to the experimental challenge of gaining noninvasive access to the interior of a random structure where light propagates.

We recently fabricated quasi-two-dimensional random waveguides to probe the transport inside from the third dimension [20,36,37]. This experimental setup has enabled us to monitor directly how the long-range spatial correlations build up inside diffusive systems [20]. Moreover, by reducing (or increasing) the width of a rectangular waveguide, we were able to enhance (or suppress) the crossing probabilities of scattering paths throughout the system and, therefore, to modify the *magnitude* of the long-range correlation function. However, the functional form of correlation remained unchanged, as it is known to be universal for diffusive waveguides with uniform width [16,18].

In this Rapid Communication, we experimentally demonstrate an effective approach of tailoring the spatial dependence of long-range intensity correlation functions *inside* a random system. This is accomplished by fabricating photonic waveguides with the cross section varying along their length. The functional form of the long-range correlation is modified inside waveguides of different shapes because the crossing probability of scattering paths is affected nonuniformly in space. Our approach enables global optimization of nonlocal effects via system geometry and it is applicable to other types of waves, such as acoustic waves and matter waves. Besides the fundamental importance, manipulating the long-range correlation of waves inside random systems is useful for imaging and focusing into multiple scattering media using wave-front shaping [10,21,38] because it affects such aspects as focusing contrast, degree of control, as well as energy deposition inside the medium. Therefore, our approach can provide an additional degree of freedom for controlling wave transport in scattering media.

To illustrate the effects of waveguide geometry on long-range spatial correlation, we first present a theoretical analysis of two-dimensional (2D) disordered waveguides. The structures have reflecting sidewalls which confine the light

*yamilov@mst.edu
†hui.cao@yale.edu

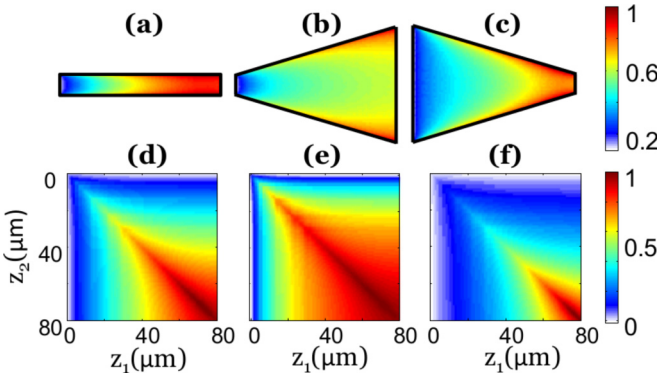

FIG. 1. (Color online) Calculated spatial long-range intensity correlation for the constant-width and two types of tapered 2D random waveguides. The waveguide length $L = 80\ \mu$m, the transport mean free path $\ell = 2.2\ \mu$m, and the diffusive absorption length $\xi_a = 26\ \mu$m. The waveguide in (a) and (d) has a constant width $W = 10\ \mu$m; in (b) and (e) $W(z)$ increases linearly from 10 to 60 μm, while in (c) and (f) $W(z)$ decreases linearly from 60 to 10 μm. (a)–(c) show the spatial distribution of the magnitude of the long-range correlation function $C_2(\mathbf{r};\mathbf{r})$ for three geometries. (d)–(f) show the long-range correlation function $C_2(z_1;z_2)$ of the cross-section averaged intensity [42] for the same geometries. The maximum value is normalized to 1 for comparison. The differences in these plots reveal that the waveguide geometry has a significant impact on the magnitude and range of C_2.

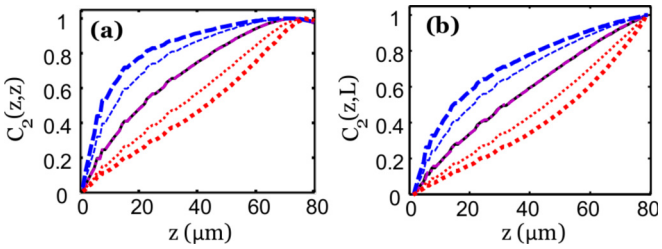

FIG. 2. (Color online) Comparison of calculated long-range correlation in six waveguides with different degrees of taper: two with constant widths of 10 μm (solid black line) and 60 μm (dashed-dotted magenta line); two with width linearly increasing from 10 μm (thick dashed blue line) or 20 μm (thin dashed blue line) to 60 μm; and two with width linearly decreasing from 60 to 10 μm (thick dotted red line) or 20 μm (thin dotted red line). Other parameters are the same as in Fig. 1. Both (a) $C_2(z;z)$ and (b) $C_2(z;L)$ clearly demonstrate that while the functional form of long-range correlation is universal for uniform waveguides, it is strongly modified in the tapered ones.

inside the waveguide where scattering and diffusion take place within the $\mathbf{r} = (y,z)$ plane, with z being the axial direction. Light transport in the random waveguide is diffusive, and the nonlocal intensity correlation is dominated by the long-range correlation C_2 [6,24]. The 2D correlation function $C_2(\mathbf{r}_1;\mathbf{r}_2)$ between two points $\mathbf{r}_1 = (y_1,z_1)$ and $\mathbf{r}_2 = (y_2,z_2)$ is calculated with the Langevin approach [18,19,39–41] (see Ref. [42] for details).

Let us consider the simplest case of linear tapering where the waveguide width $[W(z)]$ increases or decreases linearly along the waveguide axis z. Figure 1 shows the magnitude of C_2, $C_2(\mathbf{r};\mathbf{r})$ in three waveguides, with $W(z)$ being constant [Fig. 1(a)], linear increasing [Fig. 1(b)], or linear decreasing [Fig. 1(c)]. The 2D distributions of C_2 across the waveguides are clearly different in the three cases, revealing that the waveguide geometry has a significant impact on the growth of C_2. In Figs. 1(d)–1(f), the correlation functions $C_2(z_1;z_2)$ of the cross-section averaged intensity [42] further illustrate the difference: In the waveguide of increasing $W(z)$, the correlation function stays nearly constant for most values of z_1 and z_2, while in the waveguide of decreasing width, the correlation function exhibits more rapid variation over z_1 and z_2. These results suggest that the range of spatial correlation is increased (or decreased) in the gradually expanding (or contracting) waveguide, as compared to the waveguide of constant width.

For a more quantitative comparison, the magnitude of C_2 of the cross-section averaged intensity, i.e., $C_2(z;z)$, is plotted in Fig. 2(a) for six waveguides of the same length but different geometry. To compare the shapes of these curves, the maximum value of each curve is set to 1. After the normalization, the two curves for the constant widths of 10 and 60 μm coincide and agree to the universal functional form. In the expanding waveguide, $C_2(z;z)$ increases more rapidly at the beginning and levels off when light diffuses deeper into the waveguide. This is attributed to the higher crossing probability of scattering paths near the front end of the waveguide where the cross section is narrower. As the width increases with z, the crossing probability is reduced, and the enhancement of C_2 is slowed down. The contracting waveguide exhibits the opposite trend: The magnitude of C_2 grows more quickly in the second half of the waveguide due to the enhanced crossing probability. We can further conclude that by enhancing the tapering of the waveguide cross section, the change in the spatial dependence of C_2 can be made larger.

Figure 2(b) plots the correlation function $C_2(z;L)$ for two points z and L of the cross-section averaged intensity of the six waveguides studied above. After normalizing the maximum value to 1, $C_2(z;L)$ for the two constant-width waveguides coincide; in the expanding waveguide the spatial range of correlation is enhanced while in the contracting waveguide the range is reduced. To be more quantitative, we find the correlation length Δz from $C_2(L-\Delta z;L) = C_2(L;L)/2$. The constant-width waveguides have the same $\Delta z = 48\ \mu$m, whereas the waveguide tapered from 10 to 60 μm has $\Delta z = 65\ \mu$m and the one from 60 to 10 μm has $\Delta z = 27\ \mu$m. Hence, the correlation length inside the random waveguide can be tuned by geometry.

We note that the change in the functional form of the long-range correlation function cannot be explained by the effective conductance model [42]. This model, which was developed in previous studies of expanding diffusive beams inside disordered slabs [26,30], can only predict the correlations of light outside random media. Inside a random medium, the magnitude of C_2 at depth z is not determined simply by the effective conductance of the waveguide section from 0 to z, which only reflects the crossing probability of scattering paths between 0 and z. The diffusive waves that pass through z may return to it after multiple scattering and crossing in the section between z and L, thus contributing to C_2 at z as well.

Indeed, the calculated C_2 inside the random waveguide of either constant or varying cross section displays a significant difference from the prediction of the effective conductance model [42].

Next, we conduct the experiments. The 2D disordered waveguides are fabricated in a silicon-on-insulator (SOI) wafer with a 220 nm silicon layer on top of a 3 μm buried oxide. The structures are patterned by electron beam lithography and etched in an inductively coupled plasma (ICP) reactive ion etcher (RIE). Each waveguide contains a 2D random array of air holes that scatter light. The air hole diameters are 100 nm and the average (center-to-center) distance of the adjacent holes is 390 nm. The waveguide walls are made of a triangle lattice of air holes (a lattice constant of 440 nm, and a hole radius of 154 nm) that has a complete 2D photonic band gap for the in-plane confinement of light.

The monochromatic beam from a tunable cw laser source (HP 8168F) is coupled into the empty waveguide by an objective lens of numerical aperture (NA) 0.4. The light is transverse-electric (TE) polarized, i.e., the electric field is in the plane of the waveguide. After propagating through the empty waveguide, the light is incident onto the random array of air holes inside the waveguide. The front end of the random array is uniformly illuminated along the y direction. The light undergoes multiple scattering in the 2D plane of waveguide. Some of the light is scattered out of plane and imaged by a 50× objective lens (NA = 0.42) onto an InGaAs camera (Xeva 1.7-320).

From the optical image, the spatial distribution of light intensity inside the waveguide $I(y,z)$ is extracted. To smooth out the short-range fluctuations, $I(y,z)$ is averaged over the cross section of the waveguide to obtain the cross-section averaged intensity $I_v(z)$. The spatial intensity correlation $C(z_1,z_2)$ is then computed from $I_v(z)$. With the short-range contribution removed, $C(z_1,z_2)$ is dominated by long-range correlation C_2. The contribution of C_3, which is on the order of $1/g^2$ (where g is the dimensionless conductance), is negligible as $g \gg 1$ in our waveguides.

The relevant parameters for light transport in the disordered waveguide are the transport mean free path l and the diffusive dissipation length ξ_a. The dissipation results from out-of-plane scattering, which can be treated similarly as absorption [36]. From the disordered waveguides with constant width, we find $\xi_a = 26$ μm and $\ell = 2.2$ μm by fitting the measured $I_v(z)$ and $C(z_1,z_2 = z_1)$ [42]. The tapered waveguides have the same density and diameter of the air holes, and thus the values of ξ_a and ℓ are identical.

Figures 3(a) and 3(b) are the scanning electron microscope (SEM) images of an expanding waveguide and a contracting waveguide. The measured correlation functions for the cross-section averaged intensity inside the two waveguides, $C(z_1 = z,z_2 = L)$, are plotted in Fig. 3(c). The experimental data clearly show that the dependence of $C(z,L)$ on z is very different for the two tapered waveguides, which agree well to the calculation results.

Since the waveguide geometry in Fig. 3(b) is the mirror image of the one in Fig. 3(a), the $C(z,L)$ for light input from the left end of the former is equivalent to that with input from the right end of the latter. As C is dominated by the long-range

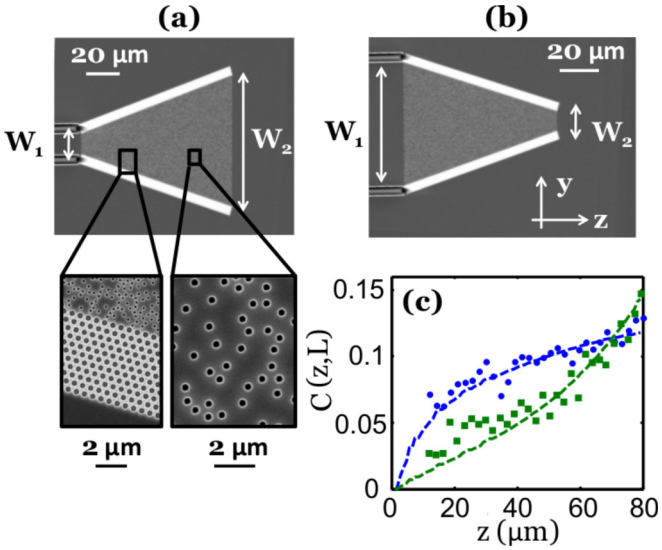

FIG. 3. (Color online) Experimental measurement of long-range intensity correlation inside the tapered waveguides. (a), (b) Top-view SEM images of fabricated quasi-2D disordered waveguides with linearly (a) increasing or (b) decreasing width. The width of the waveguide in (a) increases from 10 to 60 μm, and in (b) it is opposite. Both have the same length $L = 80$ μm. Magnified SEM images show the air holes distributed randomly in the tapered section of the waveguide and the triangle lattice of air holes in the reflecting sidewalls. (c) Measured long-range correlation function for the cross-section averaged intensity $C(z,L)$ inside the tapered waveguides shown in (a) and (b). The blue circles (green squares) represent experimental data for the waveguides with increasing (decreasing) width, and the dashed lines are theoretical results.

correlation function, this result implies C_2 becomes asymmetric. Note that the asymmetry exists only inside the random medium. The C_2 for the transmitted light remains symmetric, as it is determined by the dimensionless conductance g which has the same value for the two waveguides [42].

The difference in the correlation functions in expanding and contracting waveguides reveals that $C_2(\mathbf{r}_1;\mathbf{r}_2)$ is no longer symmetric because one waveguide is a mirror image of the other. In other words, the long-range intensity correlation function for light input from one end of the tapered waveguide is different from that with input from the other end. This behavior is distinct from that of the constant-width waveguide whose two ends are equivalent.

Next, we vary the waveguide cross section in a non-monotonic manner for further manipulation of the long-range intensity correlation inside the random waveguide. The waveguide shown in Fig. 4(a) has width W increasing linearly in the first half of the waveguide and decreasing in the second half. This geometry, unlike the tapered waveguides studied above, is symmetric with respect to the center ($z = L/2$), thus the spatial intensity correlation function is the same for light incident from either end of the waveguide. Figure 4(b) shows the spatial distribution of light intensity inside the waveguide with input from the left end. The short-range intensity fluctuations seen in Fig. 4(b) are smoothed out after the intensity is averaged over the cross section, leaving only the

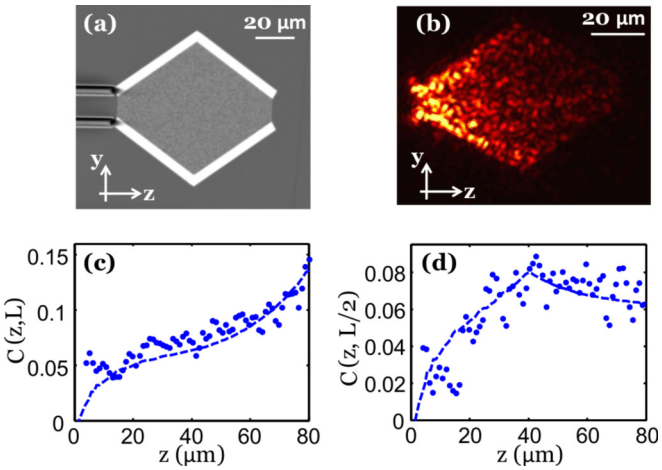

FIG. 4. (Color online) Long-range correlation in a quasi-2D disordered waveguide whose width varies nonmonotonically. (a) Top-view SEM image showing the waveguide width W increases linearly from 10 μm at $z = 0$ to 60 μm at $z = 40$ μm and then reduces linearly down to 10 μm at $z = 80$ μm. Other structural parameters are the same as the waveguides in Fig. 3. (b) An optical image of the intensity of scattered light from the disordered waveguide. The wavelength of the probe light is 1510 nm. (c) Long-range correlation function $C(z,L)$ for the cross-section averaged intensities at z and L in the waveguide shown in (a). $C(z,L)$ displays a sharp change in the growth rate before and after z passes $L/2$. (d) Long-range correlation function for the cross-section averaged intensities at z and $L/2$ in the waveguide shown in (a). $C(z,L/2)$ increases monotonically in the first half of the waveguide and decreases slightly in the second half. In (c) and (d), solid circles represent experimental data and the dashed curves are obtained by numerical calculation.

long-range contributions to the intensity correlation function $C(z_1,z_2)$. Figure 4(c) plots $C(z,L)$, which increases initially at a slow rate as z approaches $L/2$, but turns into a sharp rise once z passes $L/2$ and approaches L. This is because the crossing probability of scattering paths is first reduced as the waveguide is expanding in $z < L/2$, and then enhanced in $z > L/2$ as the cross section decreases. Therefore, the crossing probability can be controlled by modulating the waveguide width, which changes the spatial dependence of long-range correlation function. Figure 4(d) shows the intensity correlation function $C(z,L/2)$. It first increases monotonically as z moves from 0 to $L/2$, and then decreases slightly for z from $L/2$ to L. The experimental data (solid circles) are in good agreement to the theoretical results (dashed lines) in Figs. 4(c) and 4(d).

Finally, we comment that the confined geometry can be used to tailor the functional form of long-range correlations not only in real space, but also in momentum space [42]. The former sets the contrast for light focused inside a scattering medium by shaping the input wave front [15], whereas the latter determines the maximum total transmission that can be achieved with incomplete control of the input wave front [22]. Therefore, we believe our approach will have immediate applications to communication and imaging through or into turbid media [10].

We thank B. Shapiro and A. D. Stone for stimulating discussions and Michael Rooks for suggestions regarding sample fabrication. This work is supported by the National Science Foundation under Grants No. DMR-1205307 and No. DMR-1205223. The use of facilities is supported by YINQE and NSF MRSEC Grant No. DMR-1119826.

[1] P. Sheng, *Introduction to Wave Scattering, Localization, and Mesoscopic Phenomena* (Academic, Boston, 1995).
[2] E. Akkermans and G. Montambaux, *Mesoscopic Physics of Electrons and Photons* (Cambridge University Press, Cambridge, UK, 2007).
[3] A. Lagendijk, B. van Tiggelen, and D. S. Wiersma, Phys. Today **62**(8), 24 (2009).
[4] B. L. Altshuler, P. A. Lee, and R. A. Webb, *Mesoscopic Phenomena in Solids* (North-Holland, Amsterdam, 1991).
[5] M. C. van Rossum and T. M. Nieuwenhuizen, Rev. Mod. Phys. **71**, 313 (1999).
[6] R. Berkovits and S. Feng, Phys. Rep. **238**, 135 (1994).
[7] R. Pnini, in *Correlation of Speckle in Random Media, Proceedings of the International Physics School on Waves and Imaging through Complex Media, 1999, Cargese, France*, edited by P. Sebbah (Kluwer Academic, Dordrecht, 2001), pp. 392–412.
[8] S. Feng, C. Kane, P. A. Lee, and A. D. Stone, Phys. Rev. Lett. **61**, 834 (1988).
[9] S. Feng and P. A. Lee, Science **251**, 633 (1991).
[10] A. P. Mosk, A. Lagendijk, G. Lerosey, and M. Fink, Nat. Photon. **6**, 283 (2012).
[11] Z. Yaqoob, D. Psaltis, M. S. Feld, and C. Yang, Nat. Photon. **2**, 110 (2008).
[12] X. Xu, H. Liu, and L. V. Wang, Nat. Photon. **5**, 154 (2011).
[13] H. Yu, J. Park, K. Lee, J. Yoon, K. Kim, S. Lee, and Y. K. Park, Curr. Appl. Phys. **15**, 632 (2015).
[14] I. M. Vellekoop and A. P. Mosk, Phys. Rev. Lett. **101**, 120601 (2008).
[15] M. Davy, Z. Shi, and A. Z. Genack, Phys. Rev. B **85**, 035105 (2012).
[16] R. Pnini and B. Shapiro, Phys. Rev. B **39**, 6986 (1989).
[17] A. Z. Genack, N. Garcia, and W. Polkosnik, Phys. Rev. Lett. **65**, 2129 (1990).
[18] A. A. Lisyansky and D. Livdan, Phys. Rev. B **47**, 14157 (1993).
[19] J. F. de Boer, M. P. van Albada, and A. Lagendijk, Phys. Rev. B **45**, 658 (1992).
[20] R. Sarma, A. Yamilov, P. Neupane, B. Shapiro, and H. Cao, Phys. Rev. B **90**, 014203 (2014).
[21] X. Cheng and A. Z. Genack, Opt. Lett. **39**, 6324 (2014).
[22] S. M. Popoff, A. Goetschy, S. F. Liew, A. D. Stone, and H. Cao, Phys. Rev. Lett. **112**, 133903 (2014).
[23] A. Goetschy and A. D. Stone, Phys. Rev. Lett. **111**, 063901 (2013).
[24] M. J. Stephen and G. Cwilich, Phys. Rev. Lett. **59**, 285 (1987).
[25] A. A. Chabanov, M. Stoytchev, and A. Z. Genack, Nature (London) **404**, 850 (2000).

[26] T. Strudley, T. Zehender, C. Blejean, E. Bakkers, and O. L. Muskens, Nat. Photon. **7**, 413 (2013).
[27] C. P. Lapointe, P. Zakharov, F. Enderli, T. Feurer, S. E. Skipetrov, and F. Scheffold, Europhys. Lett. **105**, 34002 (2014).
[28] M. P. van Albada, J. F. de Boer, and A. Lagendijk, Phys. Rev. Lett. **64**, 2787 (1990).
[29] N. Garcia, A. Z. Genack, R. Pnini, and B. Shapiro, Phys. Lett. A **176**, 458 (1993).
[30] F. Scheffold, W. Hartl, G. Maret, and E. Matijevic, Phys. Rev. B **56**, 10942 (1997).
[31] P. Sebbah, R. Pnini, and A. Z. Genack, Phys. Rev. E **62**, 7348 (2000).
[32] P. Sebbah, B. Hu, A. Z. Genack, R. Pnini, and B. Shapiro, Phys. Rev. Lett. **88**, 123901 (2002).
[33] A. A. Chabanov, N. P. Tregoures, B. A. van Tiggelen, and A. Z. Genack, Phys. Rev. Lett. **92**, 173901 (2004).
[34] O. L. Muskens, T. van der Beek, and A. Lagendijk, Phys. Rev. B **84**, 035106 (2011).
[35] F. Scheffold and G. Maret, Phys. Rev. Lett. **81**, 5800 (1998).
[36] A. G. Yamilov, R. Sarma, B. Redding, B. Payne, H. Noh, and H. Cao, Phys. Rev. Lett. **112**, 023904 (2014).
[37] R. Sarma, A. Yamilov, T. Golubev, and H. Cao, Appl. Phys. Lett. **105**, 041104 (2014).
[38] N. Fayard, A. Cazé, R. Pierrat, and R. Carminati, Phys. Rev. A **92**, 033827 (2015).
[39] B. Z. Spivak and A. Y. Zyuzin, in *Mesoscopic Phenomena in Solids*, edited by B. L. Altshuler, P. A. Lee, and R. A. Webb (Elsevier Science Publishers, Amsterdam, 1991), Chap. 2.
[40] R. Pnini and B. Shapiro, Phys. Lett. A **157**, 265 (1991).
[41] E. Kogan and M. Kaveh, Phys. Rev. B **45**, 1049 (1992).
[42] See Supplemental Material at http://link.aps.org/supplemental/10.1103/PhysRevB.92.180203 for additional simulation results.

SUPPLEMENTARY MATERIAL
Using geometry to manipulate long-range correlation of light inside disordered media

Raktim Sarma,[1] Alexey Yamilov,[2,*] Pauf Neupane,[2] and Hui Cao[1,†]

[1]*Department of Applied Physics, Yale University, New Haven, CT, 06520, USA*
[2]*Department of Physics, Missouri University of Science and Technology, Rolla, Missouri 65409,USA*

PACS numbers: 71.55.Jv, 42.25.Bs, 72.15.Rn

CALCULATION OF LONG-RANGE INTENSITY CORRELATION FUNCTION INSIDE RANDOM MEDIA

Spatial intensity correlation function is defined by

$$C(\mathbf{r}_1,\mathbf{r}_2)=\frac{\langle I(\mathbf{r}_1)I(\mathbf{r}_2)\rangle}{\langle I(\mathbf{r}_1)\rangle\langle I(\mathbf{r}_2)\rangle}-1. \tag{S1}$$

It is a sum of three terms: C_1 responsible for short-range correlation, C_2 - the long-range correlation, and C_3 - the infinite range correlation. In the regime of diffusive transport $C_1 \gg C_2 \gg C_3$ [1] so C_3 can be safely ignored.

Expression for spatial long-range correlation function applicable for diffusive transport has been derived with the Langevin approach [2–5] from the ensemble averaged intensity $\langle I(\mathbf{r})\rangle$ and Green function $G(\mathbf{r}_1;\mathbf{r}_2)$ of diffusion equation. For a 2D geometry we find

$$C_2(\mathbf{r}_1,\mathbf{r}_2)=\frac{4}{k\ell}\frac{\int_\Omega \nabla_{\mathbf{r}'}G(\mathbf{r}_1,\mathbf{r}')\nabla_{\mathbf{r}'}G(\mathbf{r}_2,\mathbf{r}')\langle I(\mathbf{r}')\rangle^2 d\mathbf{r}'}{\langle I(\mathbf{r}_1)\rangle\langle I(\mathbf{r}_2)\rangle}, \tag{S2}$$

where $G(\mathbf{r},\mathbf{r}')$ is Green function of diffusion equation

$$\Delta_{\mathbf{r}}G(\mathbf{r},\mathbf{r}')-G(\mathbf{r},\mathbf{r}')/\xi_a^2=-\delta(\mathbf{r}-\mathbf{r}') \tag{S3}$$

with $G(\mathbf{r},\mathbf{r}')|_{\partial\Omega_o}=0$ at open boundaries and $\nabla_{\mathbf{n}}G(\mathbf{r},\mathbf{r}')|_{\partial\Omega_r}=0$ at the reflecting ones. Such boundary condition neglects surface effects which can also lead to additional terms in Eq. (S2). They are significant at $0<z\lesssim\ell$, $L-\ell\lesssim z<L$, particularly for large index mismatch between inside and outside of random medium [5]. However, in our system of air holes in dielectric, the effective refractive index of the random waveguide is less than that of the empty waveguide. In this case the effects due to surface reflection for light inside the random waveguide are not pronounced [6]. Hence our choice of boundary conditions is reasonable for our samples with $\ell \ll L$. Also, $\langle I(\mathbf{r})\rangle$ can be obtained from $G(\mathbf{r},\mathbf{r}')$ by considering a uniform source at the left boundary of the random waveguide. We note that Eq. (S2) is applicable to any 2D geometry. It reduces to the expression in Ref. [7] in the quasi-1D limit $L \gg W$. The diffusive waveguides studied in this work have $W(z) \sim L$ and are in the intermediate regime between quasi-1D and 2D ($L \ll W$) limits. In addition, we ignore the renormalization of the diffusion coefficient [8] because the localization effects are small for the waveguides studied in this work.

We use cross-section averaging to single out the C_2 contribution [7]

$$C(z_1,z_2)=\frac{\langle[1/W(z_1)]\int I(\mathbf{r}_1)dy_1[1/W(z_2)]\int I(\mathbf{r}_2)dy_2\rangle}{\langle[1/W(z_1)]\int I(\mathbf{r}_1)dy_1\rangle\langle[1/W(z_2)]\int I(\mathbf{r}_2)dy_2\rangle}-1\simeq C_2(z_1,z_2). \tag{S4}$$

Indeed, such integration suppresses the contribution from the *short-range* correlation C_1, noticeable for $|\mathbf{r}_1-\mathbf{r}_2|\sim\ell$. This is because the width of the waveguides considered in our work is always greater that transport mean free path. Using the definition Eq. (S1) we obtain

$$C_2(z_1,z_2)=\frac{\int\int\left[(C_2(\mathbf{r}_1,\mathbf{r}_2)+1)\,\langle I(\mathbf{r}_1)\rangle\langle I(\mathbf{r}_2)\rangle\right]dy_1dy_2}{\int\langle I(\mathbf{r}_1)\rangle dy_1\int\langle I(\mathbf{r}_2)\rangle dy_2}-1 \tag{S5}$$

where $C_2(\mathbf{r}_1,\mathbf{r}_2)$ is given by Eq. (S2) above.

EFFECTIVE CONDUCTANCE MODEL

An effective conductance model has been developed in the previous studies of expanding diffusive beams inside disordered slabs [9, 10]. The long-range intensity correlation function for the transmitted light is determined by the crossing probability of scattering paths inside the slab, which is on the order of $1/g$, where g is the dimensionless conductance. To account for the effect of diffuse spreading of the intensity, $1/g$ is obtained by integrating over short sections of increasing width at different depths inside the slab. While this model can predict the

long-range correlations of transmitted light, it fails inside the random medium. This is because the magnitude of long-range intensity correlation C_2 at depth z is not determined simply by the conductance of the waveguide section from 0 to z, which only takes into account the crossing probability of scattering paths between 0 and z. The diffusive waves that pass through z may return to it after multiple scattering and crossing in the section between z and L, thus contributing to C_2 at z as well.

Let us consider a simple example of a diffusive waveguide with constant width and no absorption. Since the dimensionless conductance $g(z)$ decreases linearly with depth z, $C_2(z;z) \approx 1/g(z) \approx z$ would increases linearly with z. Figure S1(a) plots the $C_2(z;z)$ calculated by the diagrammatic theory [3, 11], which displays a nonlinear increase with z. We further compare the $C_2(z;z)$ inside tapered waveguides to the prediction by the effective conductance model. As shown in Fig. S1(b, c), they differ not just quantitatively but also qualitatively. For example, the effective conductance model predicts a monotonic increase of $C_2(z;z)$ with z, the actual $C_2(z;z)$ in the tapered waveguides decreases with z near the rear end. The significant differences confirm that the changes in the functional form of the C_2 inside the random system cannot be explained by the z dependence of g.

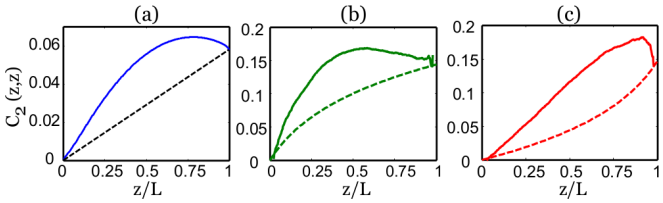

FIG. S1: (Color online) Comparison of calculated long-range correlation function $C_2(z;z)$ for the cross-section averaged intensity inside diffusive waveguides (solid line) to the prediction of the effective conductance model (dashed line). (a) The waveguide has constant width $W = 60$ μm. (b) The waveguide width increases linearly from 10 μm to 60 μm. (c) The waveguide width decreases linearly from 60 μm to 10 μm. All three waveguides have the same length $L = 80$ μm. The effective conductance model fails to predict $C_2(z;z)$ inside all three waveguides.

ADDITIONAL NUMERICAL RESULTS

In Fig. S2, we compare the $C_2(z;z)$ inside two tapered waveguides without absorption. The two waveguides are mirror image of each other, thus their difference in $C_2(z;z)$ reveals the asymmetry of long-range correlation inside the random waveguide. Nevertheless they have the same value of C_2 at the output end ($z = L$), indicating the asymmetry exists only inside the random system.

In Fig. 2 of the main text, we normalize the long-range correlation functions in order to compare their

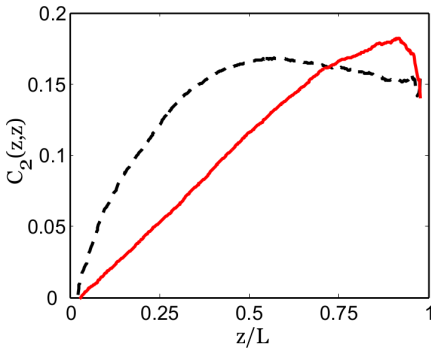

FIG. S2: (Color online) Difference in long-range correlation function between two diffusive waveguides with no absorption. (a) Black dashed curve (solid red curve) represents the calculated $C_2(z,z)$ for the cross-section averaged intensity inside a random waveguide of width tapered linearly from 10 μm (60 μm) to 60 μm (10 μm). Both waveguides have the same length $L = 80$ μm, and the transport mean free path is 2.2 μm. These two waveguides are mirror images of each other, thus their difference in $C_2(z,z)$ reveals the asymmetry of long-range correlation inside the random waveguide. Nevertheless they have the same value of C_2 at the output end ($z = L$), indicating the asymmetry exists only inside the random system.

functional form in waveguides of different size and geometry. The results confirm that the functional form of long-range correlation is modified by tapering of the waveguide. The deviation from the universal functional form in the constant-width waveguides is larger when the degree of tapering is stronger. Figure S3 shows the unnormalized $C_2(z;z)$ and $C_2(z;L)$ in four tapered waveguides and one constant-width waveguide with absorption. Their difference again illustrates the impact of the waveguide geometry on the long-range intensity correlation function inside the diffusive waveguide.

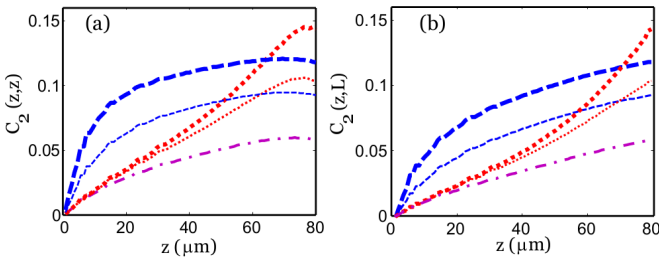

FIG. S3: (Color online) Comparison of calculated $C_2(z,z)$ (a) and $C_2(z,L)$ (b) in five waveguides with different degrees of taper: two with width linearly increasing from 10 μm (thick dashed blue line) or 20 μm (thin dashed blue line) to 60 μm; two with width linearly decreasing from 60 μm to 10 μm (thick dotted red line) or 20 μm (thin dotted red line); and one with constant width of 60 μm (dash-dotted magenta line). All the parameters are the same as in Fig. 2 of the main text.

In Fig. S4, we plot the relative difference of $C_2(z;z)$ between the two tapered waveguides where in one the width increases linearly from 10 μm to 60 μm and in the

TABLE I: Correlation length of $C_2(z;L)$ in diffusive waveguides of different geometry

Diffusive waveguide (L = 80 μm)	C_2 correlation length Δz (μm) $C_2(z, L) = C_2(L, L)/2$
W_1 = 60 μm, W_2 = 60 μm	48
W_1 = 20 μm, W_2 = 60 μm	58
W_1 = 10 μm, W_2 = 60 μm	65
W_1 = 60 μm, W_2 = 20 μm	35
W_1 = 60 μm, W_2 = 10 μm	27
W_1 = 10 μm, W_2 = 10 μm	48

other the width decreases linearly from 60 μm to 10 μm as shown in Fig. S3. The relative difference is defined as the ratio of the $C_2(z;z)$ difference to the mean. The difference is as much as 150%, illustrating the power of manipulating C_2 by geometry.

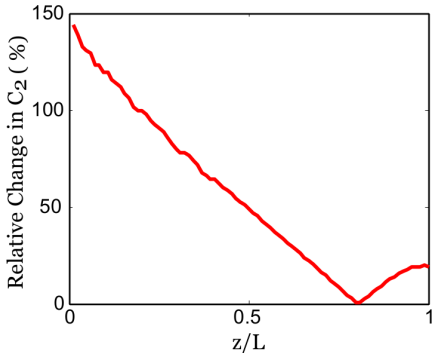

FIG. S4: (Color online) The relative difference in $C_2(z,z)$ between two tapered waveguides where in one the width increases linearly from 10 μm to 60 μm and in the other width decreases linearly from 60 μm to 10 μm as shown in Fig. S3(a). The geometry can make a difference as much as 150% in the long-range correlations.

Figure 2(b) in the main text reveals that in the expanding waveguide the spatial range of $C_2(z;L)$ is enhanced while in the contracting waveguide the range is reduced. Table I lists the correlation length Δz, defined as $C_2(L-\Delta z;L) = C_2(L;L)/2$, for waveguides of different tapering. It shows a large variation of the correlation length induced by geometry.

DETERMINATION OF SCATTERING AND DISSIPATION PARAMETERS OF FABRICATED SAMPLES

The relevant parameters for light transport in the disordered waveguide are the transport mean free path l and the diffusive dissipation length ξ_a. The transport mean free path l depends on the size and density of the air holes. The dissipation results from out-of-plane scattering as the silicon absorption at the probe wavelength is negligible. This vertical leakage of light can be treated similarly as absorption and described by the diffusive dissipation length $\xi_a = \sqrt{D\tau_a}$, where τ_a is the ballistic dissipation time and D is the diffusion coefficient [8]. The two parameters, ℓ and ξ_a, were extracted from the fitting of the measured cross-section averaged intensity, $I_v(z)$, and the magnitude of correlations $C(z,z)$ of $I_v(z)$ in a waveguide with constant width, $W = 60\mu$m and $L = 80\mu$m. The numerical calculations were done with the same method as described in the manuscript and the parameters extracted from the fitting are $\xi_a = 26$ μm and $\ell = 2.2$ μm. Figure 1(c) and (d) show the experimental data along with the fitted curves obtained from the numerical calculations.

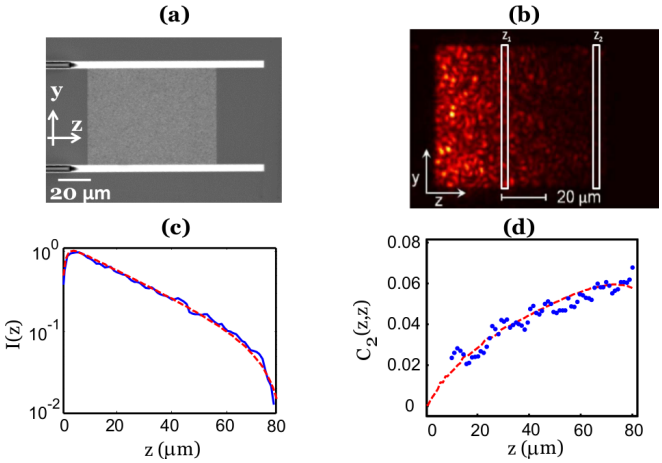

FIG. S5: (Color online) (a) Top-view scanning electron microscope (SEM) image of a quasi-2D disordered waveguide with $W = 60$ μm and $L = 80$ μm. The waveguide wall is made of a triangle lattice of air holes which forms a 2D photonic bandgap to confine light inside the waveguide. (b) An optical image of the intensity of scattered light from the disordered waveguide shown in (a). The wavelength of the probe light is 1500 nm. The white boxes mark two cross-sections at depths z_1 and z_2 in the disordered waveguide. (c,d) Fitting of experimental data to extract scattering and dissipation parameters. The solid blue line in (c) represents the experimentally measured ensemble and cross-section averaged intensity inside the waveguides shown in (a). The solid blue circles in (d) are the measured $C(z,z)$ for the cross-section averaged intensity in the waveguide shown in (a). The dashed red lines in (c) and (d) are obtained by numerical calculation with parameters $\xi_a = 26$ μm and $\ell = 2.2$ μm, which have the best fit to the experimental data.

The ensemble averaging is done over 4 random configurations of air holes and 25 input wavelengths equally spaced between 1500 nm and 1510 nm. Additional averaging is carried out by slightly moving the incident beam spot on the input facet of the empty waveguide to generate different intensity patterns with uniform envelope at the front end of the random array.

IMPACT ON LIGHT FOCUSING AND TOTAL TRANSMISSION ENHANCEMENT

In this section we present two examples to illustrate the significance of controlling long-range correlations by geometry. One example is focusing of light into a highly scattering medium, the other is enhancing total transmission through a diffusive medium.

In a numerical simulation of wavefront shaping experiment, we focus the input light to a point inside the random waveguide by adjusting the relative phase of electric field in the guided modes of the lead waveguide at the input. Then we normalize the light intensity at the focal point, $\mathbf{r} = (0, z)$, to 1, and average the intensities at all other points of the same cross-section (same z) to obtain the focusing background intensity I_b. Figure S6 plots I_b versus z in two diffusive waveguides, one tapered from 10 μm to 60 μm, the other from 60 μm to 10 μm. The variation of the background intensity with depth is dramatically different for the two waveguides, and $I_b(z)$ follows the spatial dependence of C_2 inside these two waveguides as shown in Fig. S3. Therefore, by tailoring the long-range correlation function, we are able to tune the focusing contrast via geometry. Since focusing light into a highly scattering sample by wavefront shaping opens the possibility of probing inside opaque media, our approach of controlling the quality of focusing will be important to applications of sensing and imaging into turbid media.

The wavefront shaping can also enhance the total transmission of light through a diffusive medium, but the enhancement factor is very sensitive to the fraction of input channels that can be controlled [12]. The effective degree of input control depends on the functional form of long-range correlation C_2 in momentum space, which can be changed by varying the confined geometry. Numerically we calculated the maximum transmission T_{max} that can be achieved with incomplete channel control. The enhancement of total transmission is equal to $T_{max}/\langle T\rangle$, where $\langle T\rangle$ is the mean value of total transmission. Table II lists T_{max} and $T_{max}/\langle T\rangle$ for diffusive waveguides of various shape, with only half of the input channels being controlled. Their values strongly depend on the waveguide geometry due to modification of the functional form of C_2 in momentum space.

Therefore, the confined geometry can be employed to tailor the functional form of long-range correlations not only in real space, but also in momentum space. The former sets the focusing contrast inside a scattering medium by shaping the wavefront of input light [13], whereas the latter determines the maximum total transmission that can be achieved with incomplete control of input wavefront [12]. Therefore, we expect our approach to have immediate applications to communication and imaging through or into turbid media [14].

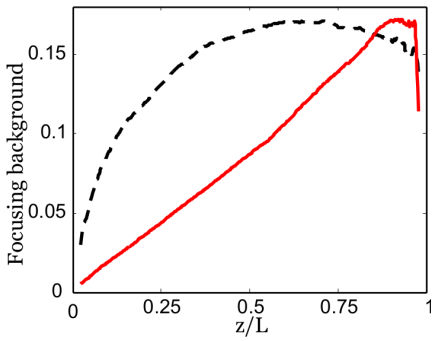

FIG. S6: (Color online) Focusing light inside a diffusive waveguide by shaping the input wavefront. The light intensity at the focal spot, $\mathbf{r} = (0, z)$, is normalized to 1. Black dashed curve (solid red curve) represents the background intensity I_b vs. depth z inside a random waveguide of width tapered linearly from 10 μm (60 μm) to 60 μm (10 μm). Both waveguides have the same length $L = 80$ μm, and they are identical to the ones shown in Fig. S3 and S4. $I_b(z)$ follows the spatial variation of C_2, as shown in Fig. S3, in both waveguides.

TABLE II: Enhancing total transmission through diffusive waveguides with different geometry by phase control of half input channels.

Diffusive waveguide (L = 80 μm)	Maximum Total Transmission	Enhancement of total transmission
W_1 = 60 μm, W_2 = 60 μm	0.57	12.8
W_1 = 60 μm, W_2 = 10 μm	0.49	27
W_1 = 10 μm, W_2 = 60 μm	0.59	5.2
W_1 = 10 μm, W_2 = 10 μm	0.47	9.62

* Electronic address: yamilov@mst.edu
† Electronic address: hui.cao@yale.edu

[1] R. Berkovits and S. Feng, *Phys. Rep.* **238**, 135 (1994).
[2] B. Z. Spivak and A. Y. Zyuzin, *Mesoscopic Phenomena in Solids*, edited by B. L. Altshuler, P. A. Lee, and R. A. Webb, (Elsevier Science Publishers, Amsterdam,

1991) Chap. 2.
[3] R. Pnini and B. Shapiro, *Phys. Lett. A* **157**, 265 (1991).
[4] J. F. de Boer, M. P. van Albada, A. Lagendijk, *Phys. Rev. B* **45**, 658 (1992).
[5] A. A. Lisyansky and D. Livdan, *Phys. Rev. B* **47**, 14157 (1993).
[6] M. C. van Rossum, and T. M. Nieuwenhuizen, *Rev. Mod. Phys.* **71**, 313 (1999).
[7] R. Sarma, A. Yamilov, P. Neupane, B. Shapiro, and H. Cao, *Phys. Rev. B* **90**, 014203 (2014).
[8] A.Yamilov, R. Sarma, B. Redding, B. Payne, H. Noh, and H.Cao *Phys. Rev. Lett.* **112**, 023904 (2014).
[9] F. Scheffold, W. Hartl, G. Maret, and E. Matijevic, *Phys. Rev. B* **56**, 10942 (1997).
[10] T. Strudley, T. Zehender, C. Blejean, E. Bakkers, and O. L. Muskens, *Nat. Photonics.* **7**, 413 (2013).
[11] E. Kogan and M. Kaveh, *Phys. Rev. B* **45**, 1049 (1992).
[12] S. M. Popoff, A. Goetschy, S. F. Liew, A. D. Stone, and H. Cao, *Phys. Rev. Lett.* **112**, 133903 (2014).
[13] M. Davy, Z. Shi, and A. Z. Genack, *Phys. Rev. B* **85**, 035105 (2012).
[14] A. P. Mosk, A. Lagendijk, G. Lerosey, and M. Fink, *Nature Photonics* **6**, 283 (2012).